Texture descriptor approaches to level set segmentation in medical images

Jimena Olveres[a], Rodrigo Nava[a], Ernesto Moya-Albor[b], Boris Escalante-Ramírez[c], Jorge Brieva[b], Gabriel Cristóbal[d] and Enrique Vallejo[e]

[a] Posgrado en Ciencia e Ingeniería de la Computación. Universidad Nacional Autónoma de México, Mexico City, Mexico
[b] Facultad de Ingeniería. Universidad Panamericana, Mexico City, Mexico
[c] Departamento de Procesamiento de Señales, Facultad de Ingeniería. Universidad Nacional Autónoma de México, Mexico City, Mexico
[d] Instituto de Óptica. Spanish National Research Council (CSIC), Serrano 121, 28006, Madrid, Spain
[e] Hospital Ángeles Pedregal. Mexico City, Mexico

ABSTRACT

Medical image analysis has become an important tool for improving medical diagnosis and planning treatments. It involves volume or still image segmentation that plays a critical role in understanding image content by facilitating extraction of the anatomical organ or region-of-interest. It also may help towards the construction of reliable computer-aided diagnosis systems. Specifically, level set methods have emerged as a general framework for image segmentation; such methods are mainly based on gradient information and provide satisfactory results. However, the noise inherent to images and the lack of contrast information between adjacent regions hamper the performance of the algorithms, thus, others proposals have been suggested in the literature. For instance, characterization of regions as statistical parametric models to handle level set evolution. In this paper, we study the influence of texture on a level-set-based segmentation and propose the use of Hermite features that are incorporated into the level set model to improve organ segmentation that may be useful for quantifying left ventricular blood flow. The proposal was also compared against other texture descriptors such as local binary patterns, Image derivatives, and Hounsfield low attenuation values.

Keywords: Hermite features, Hounsfield, Left ventricular blood flow, Level sets, Local binary patterns, Texture segmentation

1. INTRODUCTION

Due to the fact that segmentation in medical images is still a challenging problem, numerous algorithms have been proposed. Such algorithms aim to solve this important stage for the subsequent higher-level analysis. For instance, characterization of an organ in an image. Segmentation methods can be divided in a general manner into two categories: those requiring strong prior knowledge and those requiring weak or no prior knowledge. The former are more robust but require a learning phase which depends on the quality of the samples, making them less general. On the other hand, the second ones are in most cases less robust but they can be adapted to a more general scenarios.

Deformable models and their implementation by level sets proposed in[1] have been widely used in medical image segmentation.[2] Deformable models rely on the idea that a curve from a given image, subject to some constraints, can evolve in order to detect objects. According to the image features used to handle the curve evolution, they can be categorized as edge based,[3] region based[4,5] and model shape based.[6,7] An extension of

---

Further author information:
J.O.: E-mail: jolveres@uxmcc2.iimas.unam.mx
R.N.: E-mail: rodie@unam.mx

the method for vector-value images was proposed by Chan and Vese[8] and applied to color images. Additionally, Paraggios et al.[9] applied it to supervised texture segmentation problems. The vector value extension allows to introduce different kinds of features at the same time without requiring any prior knowledge. For example, Brox et al.[10] introduced simultaneously texture features, gray level and optic flow for the segmentation process.

Based on the Chan and Vese approach, we addressed the left ventricle (LV) inner wall or endocardium segmentation in order to quantify left ventricular blood flow. This is an important issue because changes of volume or flow are related to cardiac function and can imply –under certain conditions– a disease. In cardiovascular physiology, the volume of blood pumped from a heart's ventricle is generally calculated using measurements from an echo-cardiogram. The volume of blood in the ventricle at the systolic phase is subtracted from the volume of blood just prior to the beat (called end-diastolic phase). The stroke volume is a measure usually taken on the left ventricle. The left ventricular outflow view delineates the inflow and outflow tracts and is useful to assess motion of the mitral and aortic valves or septum changes in some obstructive cardiomyopathies.[11] One way to extract such a volume in cardiac computed tomography is measuring the area of the ventricle cavity for each slice created of the volume and then calculate the total volume. However, noise inherent to computerized tomographic images and the lack of contrast may hamper the final segmentation, thus, it is necessary to include more characteristics that support the algorithm decision.

Texture plays an important role in distinguishing one region from another because intensity variations may reflect different areas, shapes, or objects. Based on the fact that texture possesses spatial continuity at both local and global scales and can exhibit a large number of features, it has been widely used to perform segmentation. The occurrence of texture in an image is useful because when two or more regions meet an edge is formed. We used this fact and took advantage by using a combined approach of level sets and texture descriptors.

Heart left ventricle has a circular aspect from the short axis view. Also right and left ventricular motions can be visualized from the short axis view and it is the basis for volumetric measurements used in global ventricular function evaluation. Typical segmentation of the inner part of the ventricle includes papillary muscles which leads to an incorrect measure of the ejected volume.[12] If the final segmentation excludes most part of such muscles, specially those next to the endocardium, we could get a more precise measure of the total blood volume. We used the level set vector value approach, without any prior information, for LV segmentation in CT images, in order to propose a novel strategy that combines level sets and Hermite features that are included in the evolving equation to refine the segmentation of the endocardium wall. We also, performed an evaluation of several alternative texture descriptors.

This paper is organized as follows: in Section 2 the basic theory of level sets is presented. In Section 3 the proposal is explained, whereas in Section 4 a set of additional texture descriptors are briefly described. Section 5 is dedicated to the dataset and the experiments are shown in Section 6. Finally, we concluded this study in Section 7.

2. METHODOLOGY

Our main purpose is to obtain a segmentation of the left ventricle; we used level sets to evolve an active contour and to find a desired boundary within an image. We focused in the active contours for vector-valued images introduced by Chan and Vese where they used level sets.[8] This model is an extension of the scalar Chan-Vese algorithm that uses the sum of each component of the vector-valued image. The original definition of the algorithm is to let Ω be a bounded open subset of $\mathbb{R}^2$, with $\partial\Omega$ as the boundary. Let u_0 be a given image such that $u_0 : \Omega \rightarrow \mathbb{R}$. Let $C(s) \in [0,1] \rightarrow \mathbb{R}^2$ be a piecewise parametrized curve. This model looks for the best partition of u_0 taking only two values, namely c^+ and c^-, and with one edge C, the boundary between these two regions, characterized by $u_0 \approx c^+$ and $u_0 \approx c^-$. The object to be detected will be given by one of these regions, and the curve C will be the final boundary of the object.

The level set method defines the curvature motion and is defined with the evolving curve $C = (x,y) \in \Omega : \phi(x,y) = 0$, assuming that ϕ has opposite signs on each side of C. The vector value Chan-Vese algorithm is based on the premise that a better segmentation can be achieved using complementary information of the same image, i.e, objects with different missing parts (such as the occlusion case) or in our case with different information such

as gradients or texture. The definition of the Chan-Vese functional written in the level set form and extended to vector value is:

$$F\left(\vec{c^+}, \vec{c^-}, \phi\right) = \mu \int_\Omega \delta\left(\phi\left(x,y\right)\right) \left|\nabla\phi\left(x,y\right)\right| dxdy + \frac{1}{N}\int_\Omega \sum_{i=1}^N \lambda_i^+ \left|u_{0,i}\left(x,y\right) - c_i^+\right|^2 H\left(\phi\left(x,y\right)\right)dxdy + \ldots$$

$$+ \frac{1}{N}\int_\Omega \sum_{i=1}^N \lambda_i^- \left|u_{0,i}\left(x,y\right) - c_i^-\right|^2 \left[1 - H\left(\phi(x,y)\right)\right]dxdy \tag{1}$$

the parameters μ and $\vec{\lambda}^{+,-}$ are integral to tuning the object detector sensitivity; μ is the weight for the length term, while $\vec{\lambda}$ coefficients are the weights for the error term. In the original model, c^+ and c^- are unknown constants representing the average value of u_0 inside and outside the curve, respectively.

Taking all the components of c_i^+ and c_i^- we obtain the next equation:

$$\begin{aligned} c_i^+ &= \frac{\int_\Omega u_{0,i}(x,y)H(\phi(x,y))dxdy}{\int_\Omega H(\phi(x,y))dxdy} & \text{average } (u_{0,i} \text{ on } \phi \geq 0), \\ c_i^- &= \frac{\int_\Omega u_{0,i}(x,y)(1-H(\phi(x,y)))dxdy}{\int_\Omega H(\phi(x,y))dxdy} & \text{average } (u_{0,i} \text{ on } \phi < 0) \end{aligned} \tag{2}$$

If the minimization is performed using the Heaviside H and Dirac δ functions as specified in the original paper, we obtain the Euler-Lagrange equation:

$$\frac{\partial\phi}{\partial t} = \delta\left(\phi\right)\left[\mu\,\mathrm{div}\left(\frac{\nabla\phi}{|\nabla\phi|}\right) - \frac{1}{N}\sum_{i=1}^N \lambda_i^+\left(u_{0,i} - c_i^+\right)^2 + \frac{1}{N}\sum_{i=1}^N \lambda_i^-\left(u_{0,i} - c_i^-\right)^2\right] \tag{3}$$

this equation is implemented as a discrete model through finite differences.

The advantage of using Eq. 3 along with texture descriptors as components of an image vector is that the level set will use more information such as texture and contour that results in a better segmentation than if it uses only a single dimension of the original image.

An important step in the algorithm is to construct the vector features. Different strategies are possible; one way is to take each vector component and apply a classical Gaussian kernel. However, the major problem with this approach is the attenuation of edges due to the smoothing of Gaussian Kernels that leads to an inaccurate results. In this paper, we chose a nonlinear diffusion strategy for building the vector features that are introduced into the level set equation as in.[10]

3. THE COMBINED PROPOSAL

We propose to use the Hermite transform (HT) as texture descriptor that can be included in Eq. (3). HT is a special case of the Polynomial transform[13, 14] and analyzes pixel information using a window function $v^2(x,y)$ in order to expand the information in terms of a family of polynomials $G_{m,n-m}(x,y)$, which are orthogonal with respect to the window function. From a perceptual point of view, adjacent Gaussian windows separated by twice the standard deviation σ represent a good model of the overlapping receptive fields found in physiological experiments.[15] Therefore $v(x,y) = \frac{1}{\sigma\sqrt{\pi}}\exp\left(-\frac{x^2+y^2}{2\sigma^2}\right)$ represents a Gaussian window with a normalization factor that defines a unitary energy for $v^2(x,y)$. The HT is obtained by performing a convolution of the image $L(x,y)$ with the filter functions $D_{m,n-m}(x,y) = G_{m,n-m}(-x,-y)v^2(-x,-y)$ as follows:

$$L_{m,n-m}(x_0,y_0) = \int_{-\infty}^{\infty}\int_{-\infty}^{\infty} L(x,y)D_{m,n-m}(x_0-x, y_0-y)dxdy \tag{4}$$

where m and $(n-m)$ denote the analysis order in X and Y respectively with $n = 0, \ldots, \infty$ and $m = 0, \ldots, n$.

The associated polynomials $G_{m,n-m}(x,y)$ are defined as:

$$G_{m,n-m}(x,y) = \frac{1}{\sqrt{2^n m!(n-m)!}}H_m\left(\frac{x}{\sigma}\right)H_{n-m}\left(\frac{y}{\sigma}\right) \tag{5}$$
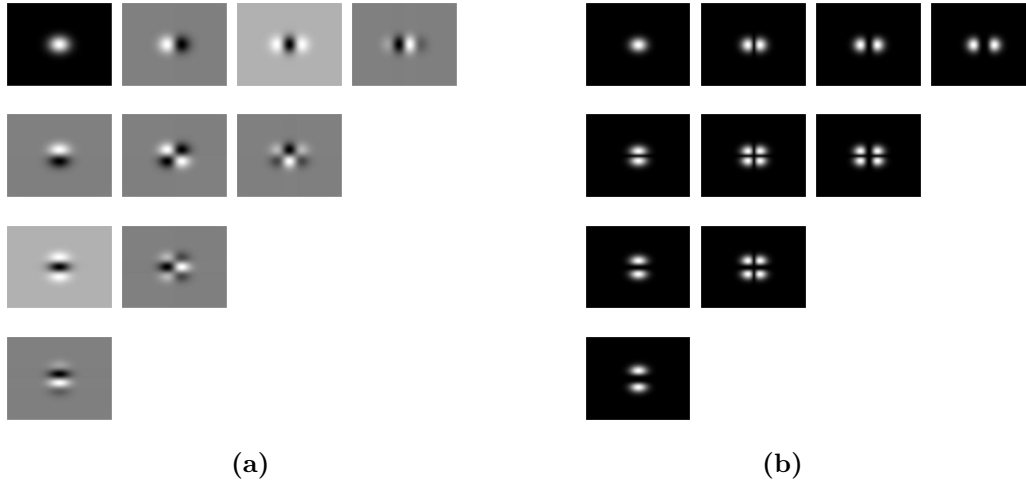
(a)   (b)

Figure 1: **(a)** An ensemble of Hermite filters of order $N = 3$ under the matrix distribution given by
$\begin{bmatrix} D_{0,0} & D_{1,0} & D_{2,0} & D_{3,0} \\ D_{0,1} & D_{1,1} & D_{2,1} \\ D_{0,2} & D_{1,2} \\ D_{0,3} \end{bmatrix}$ and **(b)** Fourier transform spectrum of the Hermite filters.

where $H_n\left(\frac{x}{\sigma}\right) = (-1)^n \exp\left(-\frac{x^2}{\sigma^2}\right) \frac{d^n}{dx^n} \exp\left(-\frac{x^2}{\sigma^2}\right)$ represents the generalized Hermite polynomials with respect to the Gaussian function (with variance σ^2). The Hermite filters are separable because the Gaussian window is rotationally symmetric and can be computed by:

$$D_n(x) = \frac{(-1)^n}{\sqrt{2^n n!}} \frac{1}{\sigma\sqrt{\pi}} H_n\left(\frac{x}{\sigma}\right) \exp\left(-\frac{x^2}{\sigma^2}\right) \tag{6}$$

An improvement of the HT is the steered Hermite transform (SHT). This transform uses filters that belong to a class of rotated filters constructed as a linear combination of the original basis.[16,17] The orientation selectivity property of the Hermite filters explains why they are products of polynomials with a radially symmetric window function (Gaussian function). The $N + 1$ Hermite filters of order n form a steerable basis for each individual filter of order n. The resulting filters can be interpreted as directional derivatives of a Gaussian function. In this way, a more general expression of the Cartesian Hermite coefficients can be written in terms of the orientation selectivity:

$$l_{m,n-m,\theta}(x_0, y_0) = \sum_{k=0}^{n} L_{k,n-k}(x_0, y_0) g_{k,n-k}(\theta) \tag{7}$$

where $l_{m,n-m,\theta}(x_0, y_0)$ are the steered Hermite coefficients and $g_{m,n-m}(\theta) = \sqrt{\binom{n}{m}}(\cos^m(\theta))(\sin^{n-m}(\theta))$ are the Cartesian angular functions of order n that express the directional selectivity of the filter.

In order to obtain the steered Hermite coefficients, the original coefficients are rotated toward the estimated local orientation, according to a criterion of maximum oriented energy at each window position, (see Figure 1). For local 1D patterns, the SHT is an efficient way to compactly describe image features into a smaller number of coefficients that represent the profile of the pattern perpendicular to its orientation (θ).[18] Since the steering angle depends on the local maximum energy, it is possible to obtain image descriptors that are invariant to the image orientation.[19]

4. OTHER TEXTURE DESCRIPTORS

We used gray level information (GRAY) as the initial feature vector and compared its performance against Hermite features. We also included in our experiments other texture descriptors such as image derivatives, local

binary patterns, and Hounsfield values as components of the feature vector. In the following paragraphs we present their description.

- *Hounsfield information.* As part of the nature of the images in cardiac computed tomography, we are interested in the attenuation values given by Hounsfield information. Such values depend on the CT attenuation method and the contrast agent. Low attenuation values of left ventricle may vary between 300 and 600 Hounsfield units (HU), thus, we propose a method that segments left ventricle by using a threshold based on Hounsfield values. Pixels between 300 and 600 HU are marked as left ventricle; otherwise are set to zero.

- *Image derivatives*[10] are used as part of a linear structure tensor that defines texture features as follows:

$$\boldsymbol{J}_0 = (\triangledown I \, \triangledown I^T) = \begin{bmatrix} I_x^2 & (I_x I_y) \\ (I_x I_y) & I_y^2 \end{bmatrix} \tag{8}$$

where I is the given image and the subscripts denote partial derivatives.

- *Uniform Local Binary Patterns* (LBPU).[20] This approach is based on the idea that textural properties within homogeneous regions can be mapped into patterns that represent micro-features. It uses a circular mask denoted by the subscript (P, R) where P is the number of sampling points around a central pixel, g_c, and R is the radius of the neighborhood, (see Figure 2). If the sampling coordinates, $(x_p, y_p) = (x_c + R\cos(\frac{2\pi p}{P}), y_c - R\sin(\frac{2\pi p}{P}))$, do not fall at integer positions then the values are bilinearly interpolated. Since over 90% of such patterns can be described with few spatial transitions that are the changes $(0/1)$ in the pattern chain, the descriptor introduces a uniformity measure $U(g_c) = |s(g_{P-1} - g_c) - s(g_0 - g_c)| + \sum_{p=1}^{P-1} |s(g_p - g_c) - s(g_{p-1} - g_c)|$ where $\{g_p | p = 0, \ldots, P - 1\}$ are the neighbors of g_c and $s(x) = \begin{cases} 1 & \text{if } x \geq 0 \\ 0 & \text{if } x < 0 \end{cases}$.

So that, the LBPU can be obtained as:

$$LBPU_{P,R}(g_c) = \begin{cases} \sum_{p=0}^{P-1} s(g_p - g_c) & \text{if } U(g_c) \leq 2 \\ P + 1 & \text{otherwise} \end{cases} \tag{9}$$
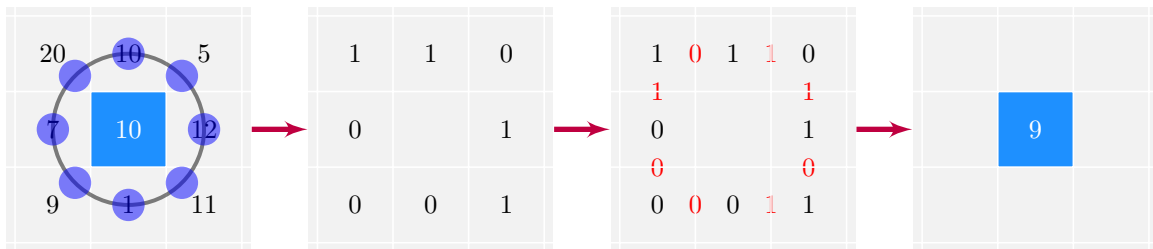

Figure 2: Based on a circular mask, the LBPU algorithm computes comparisons between a central pixel and its surrounding neighbors. In this example, the central value is $p_c = 10$ and the final label is 9.

- **BRINT**. An important disadvantage of CT images is the random noise that limits the ability of the radiologist to discriminate between two regions of different density. Since LBPs and its variants are very sensitive to noise, Liu et al.[21] proposed a simple modification based on the LBPU called Binary Rotation Invariant and Noise Tolerant (BRINT) that averages the sampling points before binarization. The authors transformed the neighbor vector in order to reduce the effects of noise, (see Figure 3).
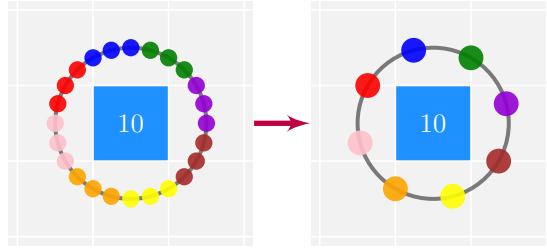
Figure 3: BRINT averages the sampling points around a central pixel before binarization. First, It transforms the original neighborhood (P=24) into a new one (P=8) by averaging the 3 adjacent neighbors to generate a binary pattern.

5. MATERIALS

We used 5 cardiac computed tomography studies from 5 different patients. Such studies were performed on a CT Siemens dual source scanner with 128 channels. Each study contains 10 volumes that correspond to time percentage of the cardiac cycle. None of them contain personal information. Originally, the volumes were not aligned with the traditional short axis view. However, the volumes need to be aligned with respect to axial and sagittal human body's axes.[11] To obtain these views it is necessary at least rotate 2 of the axes of the tomographic representation and execute a series of translations. In a mathematical form this representations are defined by 6 parameters in matrix operations: 3 for translations and 3 for rotations on the orthogonal axes. The matrix defined for translation is given by:

$$\boldsymbol{S}_{m,n} = \begin{bmatrix} 1 & 0 & 0 & xtrans \\ 0 & 1 & 0 & ytrans \\ 0 & 0 & 1 & ztrans \\ 0 & 0 & 0 & 1 \end{bmatrix} \tag{10}$$

while the matrices defined for rotations with θ radians on the X, Y, and Z axes are:

$$\boldsymbol{X}_{m,n} = \begin{bmatrix} 1 & 0 & 0 & 0 \\ 0 & \cos(\theta) & \sin(\theta) & 0 \\ 0 & -\sin(\theta) & \cos(\theta) & 0 \\ 0 & 0 & 0 & 1 \end{bmatrix}, \ \boldsymbol{Y}_{m,n} = \begin{bmatrix} \cos(\theta) & 0 & \sin(\theta) & 0 \\ 0 & 1 & 0 & 0 \\ -\sin(\theta) & 0 & \cos(\theta) & 0 \\ 0 & 0 & 0 & 1 \end{bmatrix}, \ \boldsymbol{Z}_{m,n} = \begin{bmatrix} \cos(\theta) & \sin(\theta) & 0 & 0 \\ -\sin(\theta) & \cos(\theta) & 0 & 0 \\ 0 & 0 & 1 & 0 \\ 0 & 0 & 0 & 1 \end{bmatrix} \tag{11}$$

note that the order of the matrix operations affects the result. So it is important to take it into account while transforming the volumes.

6. EXPERIMENTS AND RESULTS

In order to assess the performance of our proposal we used the SHT, namely Hermite filter, as a texture descriptor on the left ventricle endocardium. We also reviewed several texture descriptors in combination with the original image (or plain level set) that we call "GRAY." The combinations employed were: *1)* gray values belonging to the original image; *2)* Image derivatives + GRAY; *3)* Hermite filter with $N = 3$ + GRAY; *4)* Hermite filter with $N = 5$ + GRAY; *5)* Hermite filter with $N = 9$ + GRAY; *6)* Uniform LBP with (P=16,R=2) + GRAY; *7)* Multiresolution LBP with (P,R) values of (1,8), (2,16) and (3,24) + GRAY; *8)* BRINT + GRAY; and *9)* Hounsfield values + GRAY.

We compared the performance of our proposal (Hermite filters with different window sizes) with a manual segmentation along the cardiac cycle, (see Figure 4) and also included segmentation results of the descriptors previously presented in Section 4. The computation was performed using a middle slice, and each percentage of the cardiac cycle is processed sequentially, followed by sequential processing of each of our algorithms. The images for each cardiac phase are calculated independently. First, the myocardium is located by calculating the centroid of the LV blood pool on the middle slice at the first phase. Second, our algorithm is applied through all the phases.

In general we obtained a better performance using Hermite filters. Notice that the endocardial and papillary muscles are detected by applying our proposal, (see Figure 4); the boundaries are more adjusted and give the robustness needed to detect non-salient boundaries in the presence of noise. The result was a contour boundary able to enhance the structure adjustments to the endocardium walls.
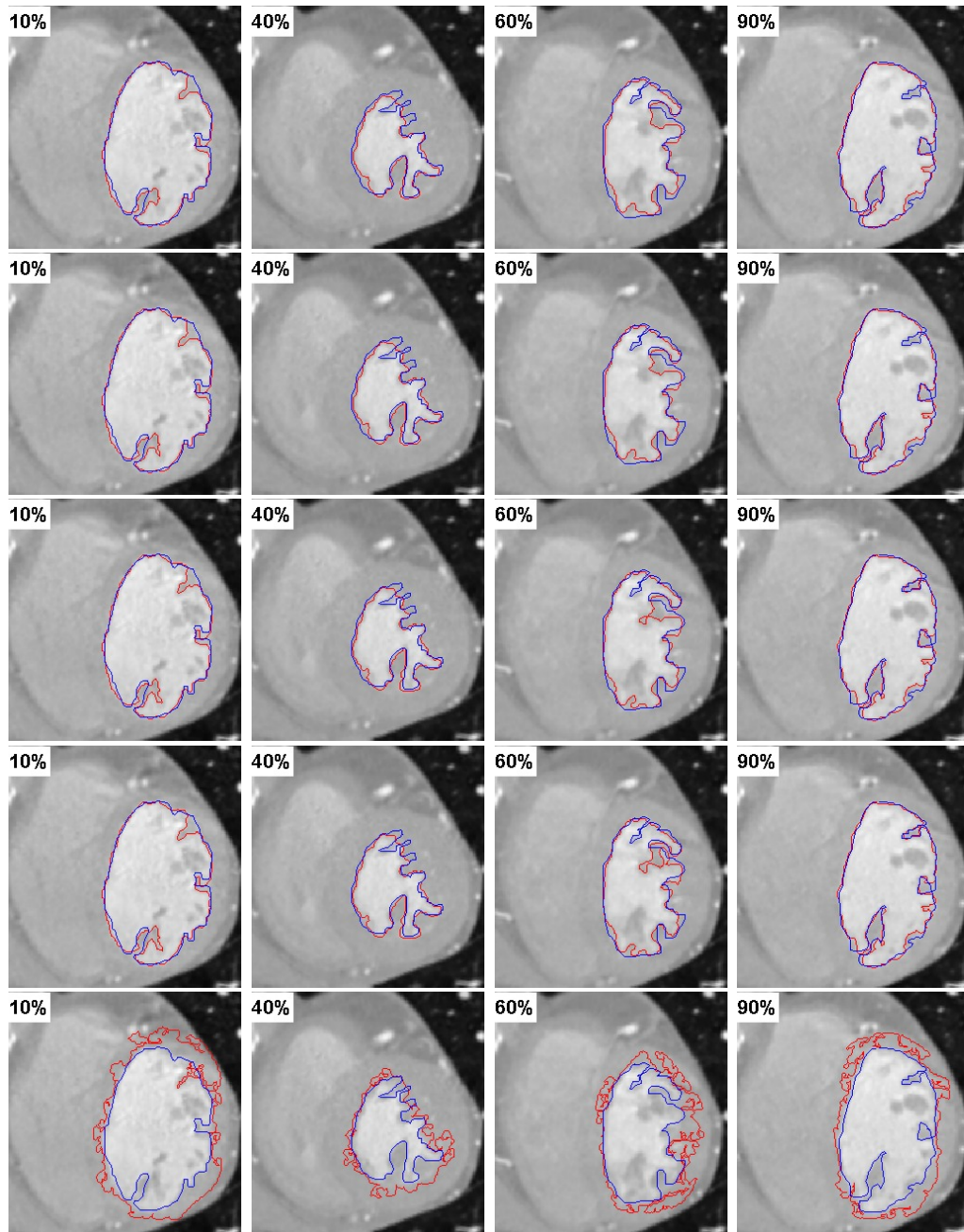

Figure 4: Segmentation comparisons between a manual contour (blue) and the level set method (red) using: GRAY **(first row)**, Hermite3 + GRAY **(second row)**, Hermite5 + GRAY **(third row)**, Hermite9 + GRAY **(fourth row)**, and LBPU + GRAY **(fifth row)**. The numbers on the images indicate the percentage of the cardiac cycle.
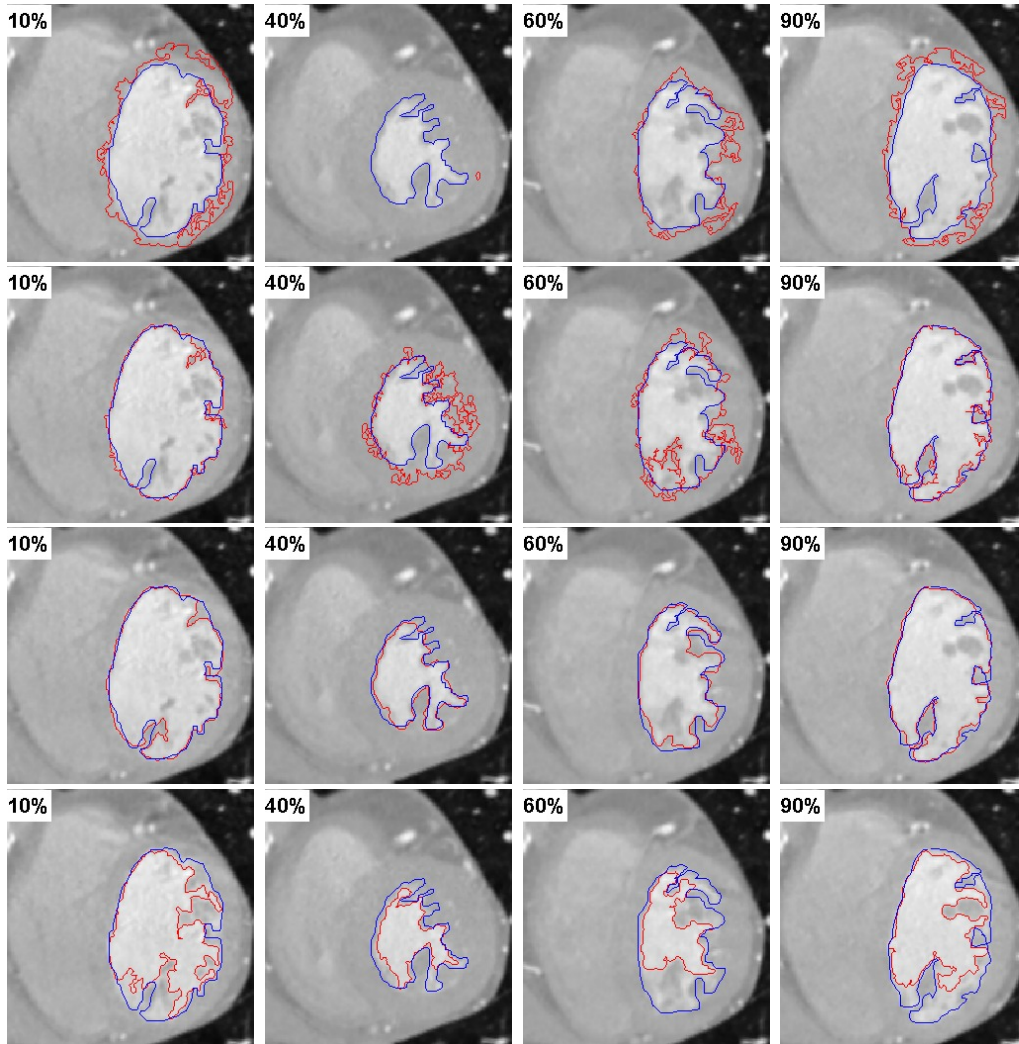
Figure 4: Continuation... Segmentation comparisons between a manual contour (blue) and the level set method (red) using: LBPUM + GRAY **(first row)**, BRINT + GRAY **(second row)**, Image derivatives + GRAY **(third row)**, and Hounsfield values + GRAY **(fourth row)**. The numbers on the images indicate the percentage of the cardiac cycle.

We also used the manual segmentation as a *ground truth* and compared it with all the methods using the Dice index and Hausdorff distance. Dice metric d_D is a measure of contour overlap given by the next equation:

$$d_D = \frac{2 \times (\|A \cap B\|)}{(\|A\| + \|B\|)} \tag{12}$$

The Hausdorff distance, d_H, measures how close a point from a first set is from another point of the second set in a metric space, in our case between two sets of points, P and Q (or boundaries). It is defined as follows:

$$d_H(P, Q) = \max\{d(P, Q), d(Q, P)\} \tag{13}$$

where $d(P, Q) = \min\{\|p_{max} - q\| \,|\, p_{max} \in \max\{\|p - q\|\}, \, q \subset Q, \, p \subset P\}$; intuitively, $d(P, Q)$ finds the p point from the set P that is the farthest from any point in Q and measures the distance from p to its closest neighbor in Q.

Table 1: Dice index results. Dice index is between 0 and 1, values close to 1 indicate more similar contours. Values 10, 20, 30, ..., represent the percentages of the CT volumes taken during the cardiac cycle. LBPUM represents a combination of three LBPUs: {P=8,R=1}, {P=16,R=2}, and {P=24,R=3}. The values represent the average index on all the patients.

Method	Cardiac Cycle (%)									
	10	20	30	40	50	60	70	80	90	100
Gray	**0.9555**	0.9354	0.9101	0.9196	0.9261	0.9005	**0.9033**	0.9268	**0.9404**	0.9362
Hermite3	0.9543	0.9484	0.9129	**0.9220**	0.9254	0.9090	0.9027	0.9333	0.9380	0.9351
Hermite5	0.9525	0.9483	0.9111	0.9208	0.9257	0.9105	0.9015	0.9337	0.9377	0.9348
Hermite9	0.9533	**0.9486**	**0.9144**	0.9218	0.9246	**0.9121**	0.8998	**0.9346**	0.9371	**0.9336**
LBPU	0.8169	0.6922	0.6303	0.7250	0.5863	0.7752	0.7823	0.6671	0.8181	0.8517
LBPUM	0.6470	0.7798	0.7446	0.5843	0.7605	0.8057	0.7860	0.8374	0.8244	0.8262
BRINT	0.7190	0.8704	0.7659	0.5656	0.7621	0.8234	0.8243	0.8466	0.8744	0.8758
Derivatives	0.9551	0.9383	0.9111	0.9205	**0.9262**	0.9063	0.9028	0.9277	0.9371	0.9359
Hounsfield	0.7228	0.6935	0.7225	0.7786	0.8366	0.7626	0.6894	0.7817	0.8354	0.7213

The results across all subjects using Dice index are shown in Table 1, while the results using Hausdorff distance are shown in Table 2. We present specific values to each percentage time of the cardiac cycle. Even we have good results in some of the experiment, notice how the values improve when we apply texture descriptors. Regarding LBPs and Hounsfield based methods, they did not work as we expected. Specially attention is taken at the ones obtained for the Hermite9 and GRAY in order to compare it.

In order to quantitatively evaluate the automatically detected endocardium, we computed the volume (blood volume) for the analyzed slide. We used all of the descriptor method results and compared them against a manual boundary contour, see Figure 5. We plotted all the cardiac cycle percentages or time phases for one patient, where the blood pool is correctly localized and distinguished. We got similar results for the rest of the patients.

Table 2: Hausdorff distance results. Lowest values indicate more alike boundaries in a range from 0 to 100. Values 10, 20, 30, ..., represent the percentages of the CT volumes taken during the cardiac cycle. LBPUM represents a combination of three LBPUs: {P=8,R=1}, {P=16,R=2}, and {P=24,R=3}. The values represent the average distance on all the patients.

| Method	Cardiac Cycle (%)									
	10	20	30	40	50	60	70	80	90	100
Gray	15.3474	16.2047	16.7948	**10.4158**	11.0670	18.3798	16.0846	20.0654	13.9249	18.4840
Hermite3	**13.7484**	**12.3431**	15.1686	10.2330	**9.2766**	**16.8456**	15.5281	19.7489	13.7101	18.6181
Hermite5	14.4327	12.9660	15.1034	11.0052	9.3024	18.1718	**15.4679**	**17.7875**	**11.4833**	**16.9516**
Hermite9	14.4082	13.1463	**13.9283**	10.8332	9.3711	18.5830	15.5381	17.9607	11.5351	20.0940
LBPU	30.9685	45.8597	38.5907	26.0963	35.1406	27.2709	25.9066	38.3039	36.4445	30.5881
LBPUM	50.3581	36.2238	28.8774	38.1228	22.4991	25.3435	27.3775	26.6793	33.2340	34.7885
BRINT	42.5114	18.7325	22.6230	44.8078	18.7936	22.5085	22.1768	19.8994	23.6611	26.6637
Derivatives	15.6608	16.0810	16.7969	10.4190	10.3948	17.1256	15.8690	19.9370	13.7082	18.4035
Hounsfield	38.7489	43.1039	32.3039	22.9846	16.0005	27.1483	39.2958	31.0560	28.4638	40.1359
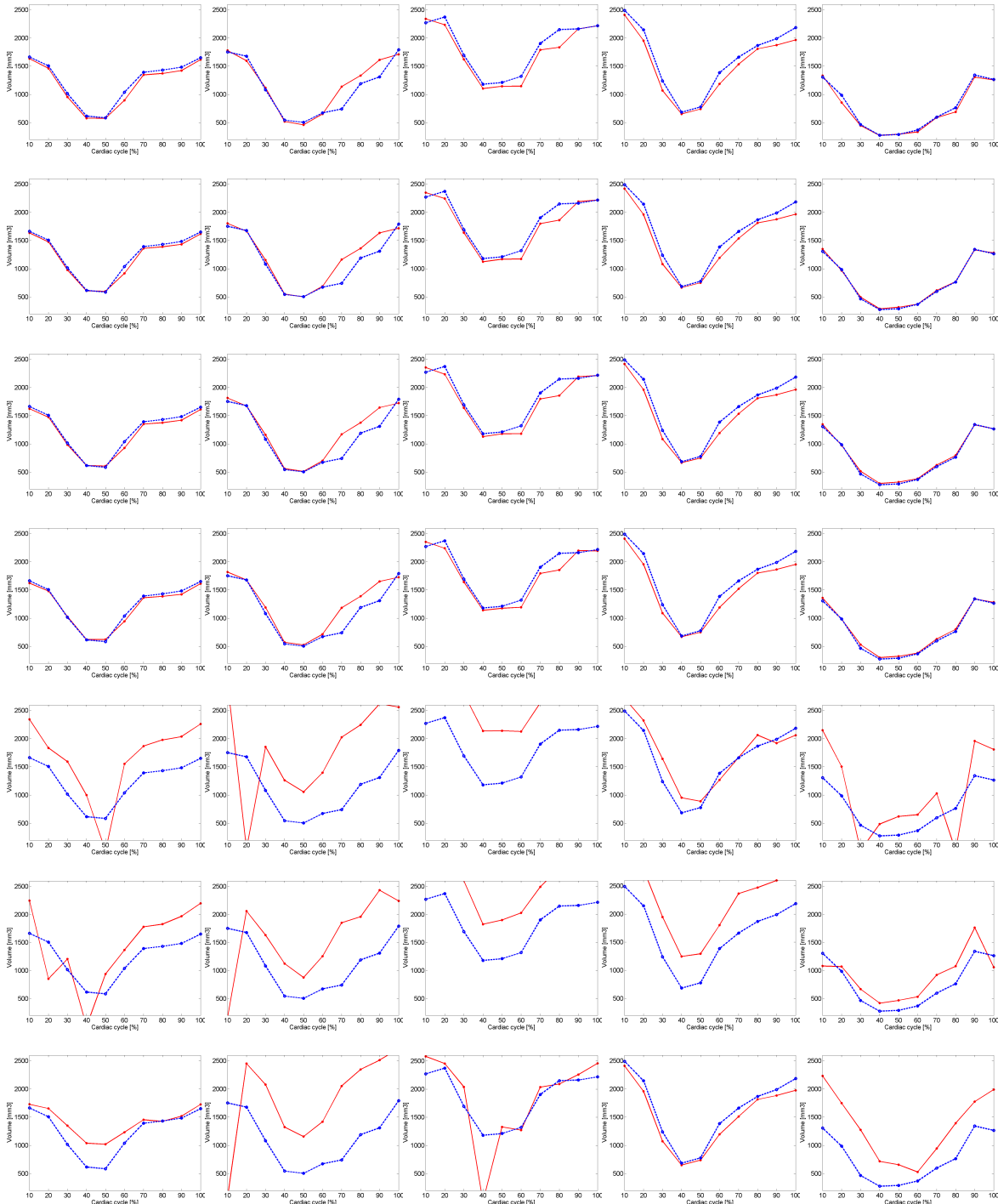
Figure 5: Left ventricle volume comparison against manual contour (blue). Each column belongs to a different patient. The methods (red) are organized as follows: GRAY **(first row)**, Hermite3 + GRAY **(second row)**, Hermite5 + GRAY **(third row)** Hermite9 + gray **(fourth row)**, LBPU + GRAY **(fifth row)**, LBPUM + GRAY **(sixth row)**, and BRINT + GRAY **(last row)**.
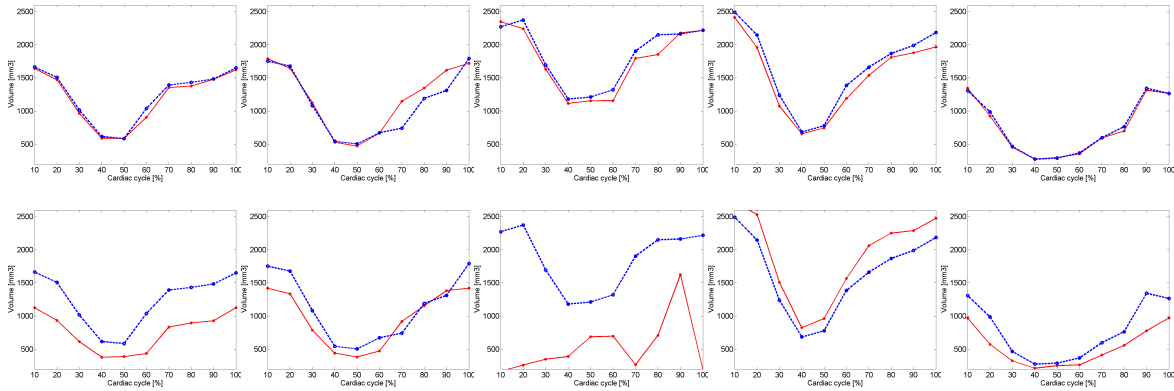
Figure 5: Continuation... Left ventricle volume comparison against manual contour (blue). Each column belongs to a different patient. The methods (red) are organized as follows: Image derivatives + GRAY (**first row**) and Hounsfield values + GRAY (**second row**).

7. CONCLUSIONS

In this work, we have implemented a semiautomatic segmentation method for the left ventricle on the short axis view through the cardiac cycle. We made use of the level set method to evolve an active contour and included texture descriptors as extra components of an image vector. The objective is to improve the boundary search by comparison by adding texture descriptors and enhance the performance. We used a bio-inspired approach using the steered Hermite transform model as one of the texture descriptors that performs a decomposition of the image into visual patterns that are relevant to the human vision system. The results achieved with the Hermite filters were more precise and detected boundaries even in the presence of noise. This study demonstrates that the proposed image segmentation algorithm accurately quantifies clinically relevant parameters such as blood volume with minimal user input. We also made use of other texture descriptors like LBPs, however, they generate a lot of information and prevent the algorithm from converging to a well defined contour.

Our proposal detects not only endocardial contours but also the papillary muscles. The segmentation of the left ventricle presented in this work constitutes a way to understanding the complex heart dynamics by segmenting the left ventricle endocardium and obtains precise quantitative measures of the heart's dynamics by taking advantage of the temporal information. Future work must be done with tasks not covered in this study such as include more patients, segment the epicardial wall as well, and also obtain the rest of quantitative LV parameters, such as ejection percentage on the whole volume, essential for all imaging techniques and significant supporting physician decisions.

ACKNOWLEDGMENTS

REFERENCES

[1] Osher, S. and Paragios, N., [*Geometric Level Set Methods in Imaging, Vision, and Graphics*], Springer-Verlag New York, Inc., Secaucus, NJ, USA (2003).

[2] Suri, J., Liu, K., Singh, S., Laxminarayan, S., Zeng, X., and Reden, L., "Shape recovery algorithms using level sets in 2-D/3-D medical imagery: a state-of-the-art review," *IEEE Transactions on Information Technology in Biomedicine* **6**(1), 8–28 (2002).

[3] Caselles, V., Kimmel, R., and Sapiro, G., "Geodesic active contours," *Int. J. Comput. Vision* **22**(1), 61–79 (1997).

[4] Chan, T. and Vese, L., "Active contours without edges," *IEEE Transactions on Image Processing* **10**(2), 266–277 (2001).

[5] Gao, S. and Bui, T., "Image segmentation and selective smoothing by using Mumford-Shah model," *IEEE Transactions on Image Processing* **14**(10), 1537–1549 (2005).

[6] Huang, C.-L., "Shape-based level set method for image segmentation," in [*Ninth International Conference on Hybrid Intelligent Systems*], **1**, 243–246 (2009).

[7] Kohlberger, T., Uzunbaş, M., Alvino, C., Kadir, T., Slosman, D., and Funka-Lea, G., "Organ segmentation with level sets using local shape and appearance priors," in [*Medical Image Computing and Computer-Assisted Intervention (MICCAI)*], Yang, G.-Z., Hawkes, D., Rueckert, D., Noble, A., and Taylor, C., eds., *Lecture Notes in Computer Science* **5762**, 34–42, Springer Berlin Heidelberg (2009).

[8] Chan, T. F., Sandberg, B. Y., and Vese, L. A., "Active contours without edges for vector-valued images," *Journal of Visual Communication and Image Representation* **11**, 130–141 (2000).

[9] Paragios, N. and Deriche, R., "Geodesic active regions: A new framework to deal with frame partition problems in computer vision," *Journal of Visual Communication and Image Representation* **13**(1-2), 249–268 (2002).

[10] Brox, T., Rousson, M., Deriche, R., and Weickert, J., "Colour, texture, and motion in level set based segmentation and tracking," *Image and Vision Computing* **28**(3), 376–390 (2010).

[11] Fischbach, R., "Cardiac and cardiothoracic anatomy in CT," in [*Multi-slice and Dual-source CT in Cardiac Imaging*], Ohnesorge, B., Flohr, T., Becker, C., Knez, A., and Reiser, M., eds., 23–39, Springer Berlin Heidelberg (2007).

[12] Lu, Y.-L., Connelly, K. A., Dick, A. J., Wright, G. A., and Radau, P. E., "Automatic functional analysis of left ventricle in cardiac cine MRI," *Quantitative Imaging in Medicine and Surgery* **3**(4) (2013).

[13] Martens, J.-B., "The Hermite transform-theory," *IEEE Transactions on Acoustics, Speech and Signal Processing* **38**(9), 1595–1606 (1990).

[14] Martens, J.-B., "The Hermite transform-applications," *IEEE Transactions on Acoustics, Speech and Signal Processing* **38**(9), 1607–1618 (1990).

[15] Sakitt, B. and Barlow, H., "A model for the economical encoding of the visual image in cerebral cortex," *Biological Cybernetics* **43**(2), 97–108 (1982).

[16] Freeman, W. T. and Adelson, E. H., "The design and use of steerable filters," *IEEE Transactions on Pattern Analysis and Machine Intelligence* **13**, 891–906 (1991).

[17] Yang, B., Flusser, J., and Suk, T., "Steerability of Hermite kernel," *International Journal of Pattern Recognition and Artificial Intelligence* **27**(4), 1354006 (2013).

[18] van Dijk, A. M. and Martens, J.-B., "Image representation and compression with steered Hermite transforms," *Signal Processing* **56**(1), 1–16 (1997).

[19] Estudillo-Romero, A., Escalante-Ramirez, B., and Savage-Carmona, J., "Texture analysis based on the Hermite transform for image classification and segmentation," *Proc. SPIE 8436, Optics, Photonics, and Digital Technologies for Multimedia Applications II, 843619 (June 1, 2012)* **8436**, 843619–843619–12 (2012).

[20] Ojala, T., Pietikäinen, M., and Mäenpää, T., "Multiresolution gray-scale and rotation invariant texture classification with local binary patterns," *IEEE Trans. Pattern Anal. Mach. Intell.* **24**(7), 971–987 (2002).

[21] Liu, L., Yang, B., Fieguth, P., Yang, Z., and Wei, Y., "BRINT: A binary rotation invariant and noise tolerant texture descriptor," in [*20th IEEE International Conference on Image Processing (ICIP)*], 255–259 (2013).